Journal of Materials Chemistry A

Accepted Manuscript

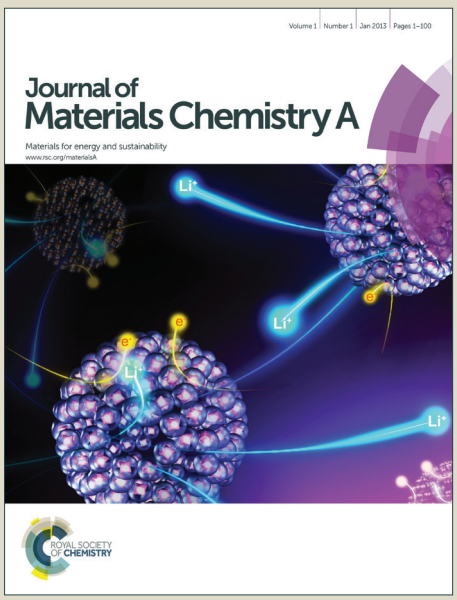

ROYAL SOCIETY OF CHEMISTRY

www.rsc.org/materialsA

Journal Name

RSCPublishing

ARTICLE

Lignosulphonate-cellulose Derived Porous Activated Carbon for Supercapacitor Electrode

Cite this: DOI: 10.1039/x0xx00000x

Zhenhuan Zhao[a,b], Shimeng Hao[b], Pin Hao[a], Yuanhua Sang[a], Ayyakkannu Manivannan[c], Nianqiang Wu[b], Hong Liu[a]**

Received ooth January 2012,
Accepted ooth January 2012

DOI: 10.1039/x0xx00000x

www.rsc.org/

The notion of environment protection and renewable sources for energy conversion and storage becomes particularly important nowadays. In this research, a meso-microporous carbon was prepared by the combination of template method and chemical activation with the earth abundant cellulose and lignosulphonate as the sources. The as-synthesized meso-microporous carbon contained mesopores generated by regeneration of cellulose and the assistance of silica template, and micropores created by chemical activation of carbon. Such unique porous structure makes the as-synthesized meso-microporous carbon be the ideal electrode active material for energy storage. The two-electrode symmetric supercapacitors built on the meso-microporous carbon electrodes shows a specific capacitance of 286 F g^{-1} at the current density of 0.25 A g^{-1} in aqueous electrolyte. More importantly, the symmetric supercapacitor achieves high energy density of 13 Wh kg^{-1} while at high power density of 27 kW kg^{-1}. It is demonstrated that using renewable natural sources as the manufacturing of porous carbon with high performance of energy storage can be an effective way to lower the cost of supercapacitor.

1. Introduction

Supercapacitors have been widely used as the energy storage means in electric vehicles,[1] wind energy farms,[2] energy management,[3] and wearable electronics.[4] Currently commercial supercapacitor electrodes are primarily made of activated carbon due to its low cost, high conductivity and good stability. The main challenge of carbon-based supercapacitors is the low energy density and non-sustainable availability of carbon source.[5] It is essential to produce activated carbon with renewable sources or recycled carbon-containing wastes. Biomass, such as coconut shells,[6] sucrose,[7] corn cob,[8] sugar cane bagasse,[9] banana peel[10] and wastes such as scrap tires,[11] has been explored to generate activated carbon for supercapacitor electrodes.

Cellulose and lignin are the largest and the second largest renewable natural carbon sources on earth, respectively.[12] In papermaking industry, cellulose is a major constituent of paper. During the pulping process, lignin is converted to lignosulphonate which is discarded as waste in black liquor.[13] Though lignosulphonate is used as dispersant, water reducing agent and manure fertilizer additive, most of them are low value-added applications. If cellulose and lignosulphonate are employed as the precursors for production of activated carbon for supercapacitors, it will convert the low-value biomass and biowaste to the high-value commercial product. Cellulose has been used as the mechanical buffer and the electrolyte reservoir for ion transport in supercapacitors,[14] or as the substrate in the form of a paper to load electrical conductive materials for flexible supercapacitors.[15, 16] Few papers have reported the conversion of cellulose to carbon as the supercapacitor electrodes. Lignin has been converted to activated carbon as the absorbent for removing contaminants or as filter for purifying air and drinking water.[17] The requirement of pore structure for absorbents and filters largely differs from that for supercapacitor electrodes.[18, 19] It is therefore important to develop a synthetic approach to convert lignin to porous active carbon that is suitable for supercapacitor electrode.

Cellulose has a large content of hydroxyl groups in its molecular structure and usually in a fiber-like morphology which consists of numerous microfibril cellulose. These microfibrils are strongly bridged with each other through hydrogen bonding.[20] As a result, cellulose can hardly be dissolved in water and some solvents, limiting its applications. NaOH/urea aqueous solution is reported to be a strong polar system and can break the hydrogen bonding to separate these microfibrils.[21] Lignosulphonate is converted from lignin and hence has much smaller molecular weight. In addition, lignosulphonate is water soluble and has a large content of reactive hydroxyl groups and aromatic rings. The reactive hydroxyl groups make lignosulphonate crosslink with other molecules such as chitosan,[22] phenol,[23] and lignosulphonate itself.[24] The crosslinked lignosulphonate has more ordered structure of aromatic rings, ensuring the high graphite degree of final carbon products.

The energy storage mechanism of the porous activated carbon-based supercapacitor electrode is built on the well-known electrical double-layer capacitance model (EDLC), in which electric energy is stored at the interface of the ultrathin double-layer between the electrode and the electrolyte.[25] The mesopores (2-50 nm in size) play an important role in the ion transport, and the micropores (less than 2 nm) are responsible for the charge storage. Therefore, it is critical to manipulate the porosity of carbon materials for improved energy storage performance. Much effort has been devoted to develop various methods to prepare porous carbons with designed porosity including core-shell ultramicroporous@microporous carbon nanospheres synthesized by time-controlled polymerization combined with KOH activation,[26] carbon foams prepared from emulsion method,[27, 28] mesoporous carbon microspheres prepared from a novel hydrothermal emulsion-activated method.[29] More impressively, microporous carbon nanoparticles without the chemical activation can be prepared.[30, 31] For example, ultramicroporous carbon nanoparticles is synthesized by solvothermal polymerization and post carbonization method.[30] Nitrogen-functionalized microporous carbon with high micropore volume can also be prepared through the direct carbonization method without activation treatment.[31] These achievements in Mingxian Liu' group provide a good methodology for the development of high performance carbon-based supercapacitors.

Take the merits of cellulose and lignosulphonate into account, in the present study, we proposed a synthetic procedure to produce meso-microporous activated carbon using cellulose and lignosulphonate as carbon sources. Cellulose is firstly regenerated to couple with the silica template. Lignosulphonate was then cast into the composites to fill voids to produce mesoporous carbon. A post chemical activation was employed to prepare meso-microporous activated carbon for the further pore structure optimization. The meso-microporous activated carbon was used to assemble symmetrical supercapacitors in aqueous electrolyte, which displays excellent electrochemical performance.

2. Experimental

2.1 Materials.

All reagents were of reagent grade and used as received without further purification. Cellulose (medium) and lignosulphonate were purchased from Sigma and Tokyochemical Industry Co., LTD, respectively. The used reagents also included cetyltrimethylammonium bromide (CTAB, Calbiochem), absolute ethanol (Macron), HCl (Alfa), NaOH (J. T. Baker), tetraethyl orthosilicate (TEOS, TCl), anhydrous $ZnCl_2$ (Alfa), super-P (Alfa), 1-methyl-2-pyrrolidinone (NMP, Sigma), and polyvinylidene fluoride (PVDF, Sigma).

2.2 Synthesis of meso-microporous activated carbon

Meso-microporous activated porous carbon (MAPC) was prepared through the following four steps including (i) cellulose regeneration, (ii) silica template preparation, (iii) lignosulphonate impregnation and carbonization, and (iv) silica template removal and chemical activation. The typical preparation process is illustrated in Figure S1. First, to regenerate cellulose, 1 g of cellulose was added into 100 mL of the NaOH/urea solution containing 6 g NaOH and 4 g urea under stirring. The mixture was then frozen at -12 ^{o}C for 12 h to completely dissolve cellulose. The frozen sample was thawed and mixed with a 5 wt% H_2SO_4 aqueous solution, and then held at ambient temperature for 10 min. The regenerated cellulose was collected and washed with copious deionized water through filtration until a neutral pH reached. Second, the regenerated cellulose was dispersed into a 100 mL of solution containing 2.4 g of CTAB, 0.2 g of NaOH, and 20 mL of absolute ethanol. After stirred at 40 ^{o}C for 12 h, 2.5 mL of TEOS was added and kept stirring at 40 ^{o}C for 6 h. The white product was collected and washed with ethanol and deionized water several times to fully remove the residual CTAB, followed by drying process in air overnight. Third, lignosulphonates were cast into the silica template. This process was repeated twice to ensure full filling of lignosulphonate in the voids of silica template. Then, the mixture was carbonized at 900 ^{o}C in N_2 gas for 3 h. The silica template was removed by immersing the carbonized product into a 2.5 M NaOH solution for 12 h, followed by washing treatment and drying process. Fourth, the carbon product was mixed with $ZnCl_2$ with a various mass ratios of $ZnCl_2$ to carbon (1:1, 1:3 and 3:1). The mixture was activated in N_2 in a tube furnace at 900 ^{o}C for 2 h. The activated carbon was washed with 1 M HCl and deionized water. The product was then dried at 70 ^{o}C to obtain the meso-microporous activated carbon, note as HAPC-XX-YY, where XX is the mass ratio of $ZnCl_2$ to carbon, and YY is the activation temperature in Celsius.

For complete comparison, another four kinds of carbon samples were also prepared. The preparation of regenerated cellulose-lignin-derived carbon (LRCC) was similar with the procedure to MAPC except that chemical activation was not performed. Pure cellulose without any treatment was directly carbonized in N_2 at 900 ^{o}C for 3 h to obtain cellulose-derived carbon (CC). Regenerated cellulose was also carbonized under the same condition to obtain the regenerated cellulose derived carbon (RCC). Pure cellulose without regeneration was used to load the silica template in a similar procedure to HAPC. However, no chemical activation was performed on the cellulose-lignin-derived carbon (LCC).

2.3 Microstructure characterization.

The morphology of the as-prepared samples was examined using a JEOL 7600F scanning electron microscopy (SEM). The porous structure was observed under a JEOL 2100F transmission electron microscopy (TEM). The chemical structure was characterized using a PHI 5000 Versa Probe X-ray photoelectron spectroscopy (XPS). Raman spectra were acquired using Renishaw Raman spectroscopy. Fourier transform infrared spectroscopy (FTIR) was performed with a NEXUS 870 spectrometer. The porous characteristics of carbon were measured by N_2 adsorption/desorption experiments at 77 K using ASAP 2020 V3.02 H. The specific surface area was measured according to the Brunauer-Emmett-Teller (BET) method and the pore size distribution was calculated using a slit pore non-local density functional theory (NLDFT) model.

2.4 Electrochemical measurements.

Both the three-electrode and the two-electrode configurations were employed to evaluate the electrochemical performance of

carbon samples. In the three-electrode set-up, A 6 M KOH aqueous solution was used as the electrolyte. A platinum gauze and the Ag/AgCl electrode were used as the counter electrode and the reference electrode, respectively. The working electrode was fabricated by physically mixing as-synthesized active carbon materials, super-p (commercial carbon black) and PVDF with a mass ratio of 8:1:1. The PVDF was previously dissolved in NMP. The mixed slurry was cast onto a nickel foil with a coverage area of about 1 cm^2, and then the nickel foil was dried at 70 ^oC for 12 h to remove the organic solvent. In the two-electrode cell, the working electrode was prepared by the same procedure while the nickel foil was replaced with the nickel foam. To ensure the same loading of the active carbon, several pieces of nickel foams were used, and those with the same loading amount of active carbon were chosen to assemble the two-electrode symmetric supercapacitor. A laboratory qualitative filter paper was used as the separator. A 6 M KOH aqueous solution was used as the electrolyte.

Cyclic voltammetry (CV), electrochemical impedance spectroscopy (EIS) and constant galvanostatic charge/discharge tests were conducted with a Gamry Reference 3000^{TM} instrument. The CV measurement in the three-electrode configuration was performed at a potential window of -1 to 0 V versus Ag/AgCl while the potential window in the two-electrode cell was 0~0.8 V. The EIS measurement was performed at an AC amplitude of 5 mV in a frequency range from 0.01 Hz to 1 MHz. The specific capacitance from CV curves collected from the three-electrode tests was calculated by $C = \int Idt/mV$. Where I is the current, V is the voltage window and m is the mass of the material at each working electrode. The integrating process was performed by Echem Analyst software. The specific capacitance was calculated from the galvanostatic discharge curve according to Equation of $C= Idt/mV$. Where I is the discharge current, t is the discharge time, V is the voltage window and m is the mass of active material at each electrode. The specific capacitance derived from the CV curve and galvanostatic testing was determined by $C=4 \int Idt/MV$ and $C=4It/mV$, respectively, where M is the total mass of material at the two-electrodes. The energy density (E) and the power density (P) were calculated from galvanostatic charge/discharge testing by equations of $E=CV^2/2$ and $P=E/t$, respectively, where C is the specific capacitance from the two-electrode tests and t is the discharge time

3. Results and discussion

The morphology of the composite containing silica nanoparticles and cellulose fiber was observed by SEM, as shown in Figure S2. It can be seen that the cellulose fiber have very large diameter and its surface was covered by silica nanoparticles. Figure S3 shows the SEM images of CC, LCC and LRCC. It can be seen that the CC sample prepared from the carbonization of pure cellulose displays irregular fiber-like morphology. These carbon fibers have very smooth surface and very large diameter in the scale of several micrometers. The LCC sample also displays fiber-like morphology similar with that of CC sample and very rough surface decorated with numerous carbon nanoparticles, which means that mesoporous carbon is successfully prepared with the assistance of silica nanoparticles. Interestingly, the LRCC sample displays totally different morphology compared with those of CC and LCC. The fiber-like morphology is disappeared and numerous carbon nanoparticles are formed. The reason is attributed to the cellulose regeneration. NaOH/urea system is commonly used to dissolve cellulose. It is reported that the alkali hydrates, urea hydrates and free water can penetrate into the voids of microfibril celluloses and destroy the intra- and inter- hydrogen bonds to separate these microfibril celluloses with each other.[32] These microfibril celluloses was regenerated by adding 5 wt% H_2SO_4. As reported, the formation of the silica nanoparticles is ascribed to the hydrolysis-condensation mechanism of TEOS. [33, 34] There are three typical growth stages of silica nanoparticles. The first stage is the monomer addition growth involving nucleation and nucleus growth; the second stage is the controlled aggregation of sub-nanoparticles which is influenced by time and the concentration of TEOS; the last stage is the formation of a layer of tight aggregated particles covering the surface of silica nanoparticles formed in the second stage. The final silica nanoparticles are then covered by positively charged CTA^+ cations thereby preventing the aggregation of silica nanoparticles, allowing the formation of a stable colloidal silica. For the cellulose without regeneration, some of the silica nucleus are assembled onto the surface cellulose to form silica nanoparticles, as can be seen in Figure S2. For the regenerated cellulose, the added TEOS can penetrate into the voids of microfibril cellulose network and finally to form silica nanoparticles. The size of the silica nanoparticles is affected by the concentration of TEOS and hydrolysis-condensation time. In this study the used time is as long as 6 h, which is far longer than that in literatures.[33] Therefore, silica nanoparticles with larger size are expected, which are stabilized by CTA^+. As a result, numerous voids are formed among these silica nanoparticles to form the mesoporous template. Later, the added lignosulphonate molecules can fill in the voids. Through carbonization and removal of silica nanoparticles, mesopores are formed. Therefore, cellulose regeneration and silica nanoparticles can be combined to prepare mesoporous carbon materials.

In order to further optimize the porosity of LRCC, a post chemical activation was employed on the LRCC sample. Figure 1 shows the SEM and TEM images of the meso-microporous activated carbon (HAPC-11-900). Seen from the SEM image, compared with LRCC, the HAPC-11-900 sample consists of more uniform carbon nanoparticles. These carbon nanoparticles are interconnected to form numerous voids between them. Figure 1b shows the TEM image of HAPC-11-900. For comparison, the TEM image of LRCC before chemical activation is illustrated in Figure S4. Both the LRCC and HAPC-11-900 display a porous structure with numerous mesopores. However, the micropores are barely observed in the HRTEM image. The difference of pore structure is hard to be observed in the present TEM image of the samples before and after chemical activation. There, nitrogen adsorption/desorption measurement was performed on the as-prepared samples. The isotherm curves and pore distribution of these samples are displayed in Figure S5. The profiles of all the isotherm plots of these carbon samples are found to be of type IV isotherm curves, suggesting the dominant mesoporosity.[34]

Obviously, for the activated carbon samples, the hysteresis loops at a relative pressure of 0.5-1.0 is the typical feature of type H4 hysteresis loop, indicating the hierarchical pore structure consisting of micropores and mesopores.[35] The size of mesopores and micropores are mainly centered at 2.5 nm and 0.7 nm, respectively.

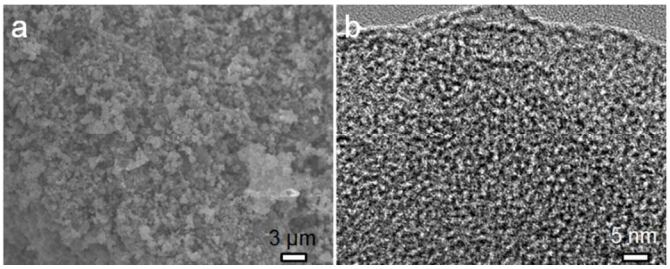

Figure 1. (a) SEM and (b) TEM images of the meso-microporous activated carbon sample (MAPC-11-900).

Table 1 summaries the specific surface area, pore volume and size, specific surface capacitance and rate capability of these carbon samples. The CC has the lowest mesopore volume, however, the mesopore volume of LCC increases to 0.18 cm^3 g^{-1}, indicating the successful introduction of mesopores by the aid of silica template. The specific surface area of LCC is about 260 m^2 g^{-1} and increases to about 426 m^2 g^{-1}, confirming the regeneration process is an effective way to increase the specific surface area. It can be also found that the activated carbon samples typically has much higher specific surface area and total pore volume than LRCC without chemical activation. The reason can be ascribed to the chemical activation process. In the present study, in order to optimize the pore structure by opening the as-formed closed pores and introducing micropores, $ZnCl_2$ activation is employed, which is demonstrated to be very efficient. During the chemical activation process, $ZnCl_2$ not only etches the carbon with lower graphite degree to open closed pores, but also creates micropores.

Table 1. The specific surface are, pore volume and size, specific capacitance and rate capability of the as-prepared carbon electrodes.

Sample ID	Surface area (m^2 g^{-1})	Total pore volume (cm^3 g^{-1})	Micropore volume (cm^3 g^{-1})	Mesopore volume (cm^3 g^{-1})	Micropore median size (nm)	Mesopore median size (nm)	Specific capacitance C_s (F g^{-1})	Rate capability R_c
Variable	X_1	X_2	X_3	X_4	X_5	X_6	C_s	R_c
CC	156	0.03	-	0.03	-	-	39	0.27
LCC	260	0.21	0.03	0.18	0.76	4.68	119	0.42
LRCC	426	0.29	0.07	0.22	0.75	5.11	165	0.35
HAPC-11-800	694	0.45	0.10	0.35	0.78	4.61	149	0.97
HAPC-11-700	740	0.47	0.17	0.30	0.76	4.37	150	0.78
HAPC-13-900	743	0.57	0.05	0.52	0.78	4.03	170	0.95
HAPC-11-900	856	0.58	0.17	0.41	0.76	5.83	246	0.79
HAPC-31-900	858	0.64	0.08	0.56	0.77	4.45	130	1.35

Note: The specific capacitance C_s is defined as the capacitance obtained at scan rate of 2 mV s^{-1}. The rate capability R_c is calculated as the ratio of the prepared capacitance value at 100 mV s^{-1} to that at 2 mV s^{-1} using three-electrode configuration.

It is noted that HAPC-11-900 sample has the highest micropore volume of about 0.17 cm^3 g^{-1} with the specific surface area as high as 856 m^2 g^{-1}.

The chemical structure of the as-prepared carbon samples was investigated using X-ray photoelectron spectroscopy (XPS) and Fourier-transform infrared spectroscopy (FTIR), as shown in Figure S6 and Figure S7, respectively. According to the results of XPS, there are only two peaks of C1s and O1s for all the carbon samples. Oxygen existed in the carbon samples in the form of –C-OH and C=O, which was confirmed by the C1s core-level peak at 286.0 eV and 287.0 eV, respectively.[36] The –OH group was also confirmed by the FTIR band at 3450 cm^{-1} in Figure S7. The FTIR bands at around 1637 cm^{-1} were indexed to benzene ring skeletal vibration.[37] For carbon materials, the graphite degree can be revealed by Raman spectra. Figure 2 displays the Raman spectra of LCC, LRCC and HAPC-11-900. The Raman spectra of CC and RCC is shown in Figure S8. For all the as-prepared carbon samples, there are three peaks located at 1350 cm^{-1}, 1580 cm^{-1} and 2790 cm^{-1}, respectively. These three peaks can be assigned to the D band originated from the vibration of disordered sp^3 carbon, and G band originated from the vibration of ordered sp^2 carbon, as well as the 2D band which is the characteristic of graphite carbon.[38] The intensity ratio of I_D/I_G indicates the graphitization degree, defects or the domain size of graphitization.[39, 40] In general, graphitization degree has an inverse relationship to the intensity ratio of I_D/I_G. The intensity ratio of I_D/I_G for CC, RCC, LCC, LRCC and HAPC-11-900 is calculated to be 0.95, 0.87, 0.88, 0.89 and 0.87, respectively. The highest value of 0.95 for CC indicates the lowest graphitization degree, while the very low similar value for RCC, LCC, LRCC and HAPC-11-900 demonstrates the very high graphitization degree of these carbon samples. The dissolution and regeneration process transforms the amorphous cellulose to crystallized cellulose.[41] The ordered microfibril structure and higher density of the crystalline cellulose promote the formation of ordered carbon in the RCC sample. In addition, there is benzene ring in lignosulphonate and it is easily crosslinked to form network structure with ordered benzene. These properties of lignosulphonate facilitate the formation of pseudo graphene structure in the final carbonized material, leading to a low I_D/I_G value of carbon materials prepared from lignosulphonate. As a result, carbon samples prepared from lignosulphonates (LCC, LRCC and HAPC-11-900) have lower ratio of I_D/I_G, compared with cellulose derived carbon (CC). Since these carbon samples already have high graphitization degree, the $ZnCl_2$ activation did not significantly improve the graphite degree by etching the poorly graphitized carbon. Lignosulphonate typically has two types of hydroxyl groups.[42] One is connected to the alkane chain and the other to the aromatic ring (phenolic hydroxyl group). These hydroxyl groups are reactive and can be crosslinked with each other through

hydrogen bond. It is believed that during the impregnation and drying process one phenolic hydroxyl group forms two hydrogen bonds with two hydroxyl groups in the alkane chains of two lignosulphonate, as illustrated in Figure S9. The crosslinking reaction bridges the lignosulphonate molecules to form a network with ordered arrangement of aromatic rings, which facilitates the formation of highly graphitized carbon.

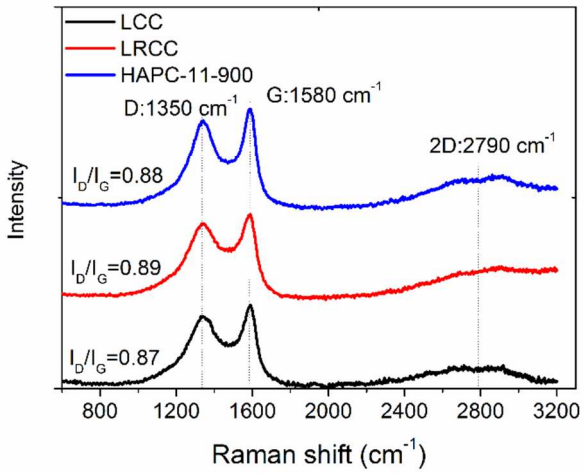

Figure 2. Raman spectra of LCC, LRCC and HAPC-11-900.

Cyclic voltammetry (CV) was used to evaluate the electrochemical performance of the as-prepared carbon samples with a three-electrode electrochemical cell in a 6 M KOH aqueous electrolyte, as shown in Figure 3. Generally, ideal electrochemical active electrode material has nearly rectangular CV shape.[43] The CV profiles of CC and RCC shows triangle shape (Figure 3a and 3b), indicating their poor supercapacitive behaviour. After the introduction of mesoporous structure with the assistance of mesoporous silica template, the CV curves of LCC and LRCC is approaching to rectangular shape, indicating the improved supercapacitive performance of LCC and LRCC. Surprisingly, nearly symmetrical box-like shape of CV curves of the HAPC-11-900 sample can be seen from Figure 3e, demonstrating the ideal supercapacitive performance. Figure 3f summarized the specific capacitance of the CC, RCC, LCC, LRCC and HAPC-11-900 according to the CV testing. The specific capacitance at 2 mV s^{-1} of CC, RCC, LCC, LRCC and HAPC-11-900 is about 39 F g^{-1}, 80 F g^{-1}, 119 F g^{-1}, 165 F g^{-1} and 246 F g^{-1} respectively. The HAPC-11-900 sample shows the highest specific capacitance. This means by careful control over the porous structure of carbon materials the electrochemical performance can be significantly improved. The reason is ascribe to the best physical properties of HAPC-11-900. As shown in Table 1, the carbonized cellulose (CC), the lignosulphonate-cellulose (LCC) and the lignosulphonate-regenerated cellulose (LRCC) possess much lower specific surface area, compared with the activated sample. But the volume ratio of mesopores to micropores varied with both the activation temperature and the mass ratio of $ZnCl_2$ to carbon. It should be pointed out that over-activation occurs when increasing the mass ratio of $ZnCl_2$ to carbon to 3:1 (HAPC-31-900). During the activation process, several adjacent micropores collapse and the walls break, and connect the micropores together to form one mesopore, which should explain why the micropore volume decreases and the mesopore volume increases for the HAPC-31-900 sample. The resulted different electrochemical performance are shown in Figure S10. The only difference among these activated carbon samples is the current density. It is found that HAPC-11-900 electrode displays the highest current density at all scan rates, confirming the best electrochemical performance of HAPC-11-900.

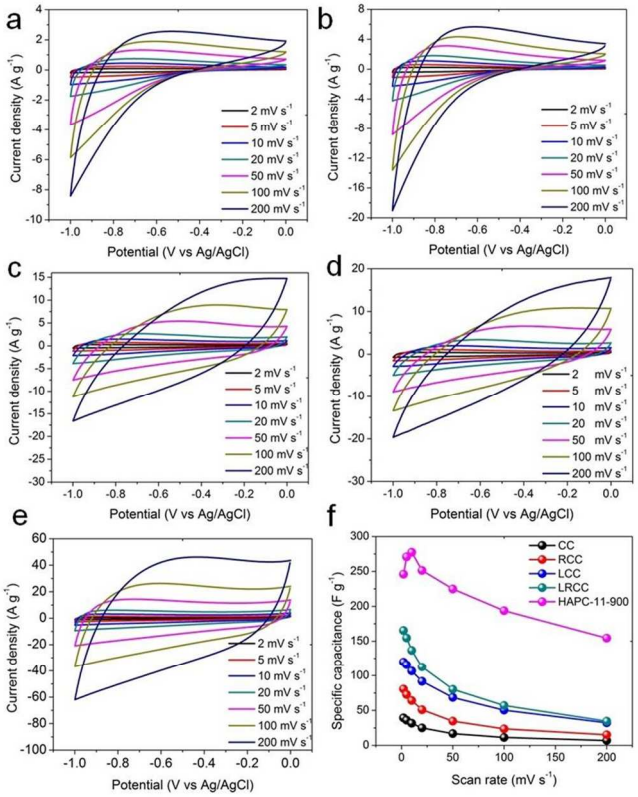

Figure 3. CV profiles of as-prepared carbons (a) CC, (b) RCC, (c) LCC, (d) LRCC and (e) A-LRCC. (f) shows the specific capacitance as a function of scan rate for CC, RCC, LCC, LRCC and ALRCC.

The energy storage ability of carbon materials is highly related to the porous structure. It is reported that different type of pores plays different role and has different contribution to energy storage. Generally, micropores (lower than 2 nm) have the largest contribution to energy storage, and mesopores (2-50 nm) are mainly responsible for electrolyte ion transportation. Macropores are usually thought to be the ion reservoir. Here, we used linear correlation analysis to investigate the relationship between the pores and electrochemical performance using the data listed in Table 1. Linear correlation analysis is an effective way to study the relationship among multi variables.[11, 44] The Correlation can be calculated using the following equation if there exists a linear relationship.

$$C(x,y) = \frac{n\sum(xy) - \sum x \cdot \sum y}{\sqrt{[(n\sum x^2 - (\sum x)^2) \cdot ((n\sum y^2 - (\sum y)^2)]}}$$

Where C is the correlation, x and y are the two variables, n is the number of variable x or y. If the value of C is larger than 0.8, x and y are highly related; if the value of C locates between 0.5 and 0.8, x and y is medially related; if C locates between 0.3 and 0.5, x and y has low relationship and no relationship if lower than 0.3.

We found that the specific capacitance Cs has a linear relationship and can be fitted as $C_s = 76.4 + 892\ X_3$ with R^2 of about 65%. The rate capability R_c and mesopore volume X_4 also have linear relationship and can be expressed using the equation $R_c = 0.19 + 1.6X_4$ with R^2 of about 72%. The calculated correlation $C(X_1, X_3)$ and $C(X_2, X_3)$ is 0.77 and 0.71, respectively, located between 0.5 and 0.8. This indicates that the specific surface area (X_1) and total pore volume (X_2) is medially related to mesopore volume (X_3). In other word, micropore volume has high effect on the specific surface area and total pore volume. The correlation $C(X_3, R_s)$ and $C(X_4, R_c)$ is calculated to be 0.85 and 0.83, indicating the micropore volume is highly related to the specific capacitance and the mesopore volume is highly related to the rate capability.

The HAPC-11-900 samples has been shortlisted to be the sample with the best electrochemical performance. Compared to a three-electrode cell, a two-electrode cell reflects the electrochemical performance of supercapacitor in practice.[45] Therefore, a two-electrode symmetric supercapacitor was assembled with HAPC-11-900 as the electrode material in the 6 M KOH aqueous electrolyte, as shown in Figure 4. In Figure 4a, the CV profiles of the symmetric supercapacitor shows ideal symmetric rectangular shape, indicating the high quality of the prepared electrode and ideal electrochemical performance of HAPC-11-900. The Nyquist plot obtained from the two-electrode cell in Figure 4b can be fitted with the equivalent circuit model in Figure S11.The ohmic resistance and the charge transfer resistance were estimated to be 2.2 Ω and 3 Ω, respectively. Figure 4c shows the plots of the imaginary capacitance (C_{image}) and the real capacitance (C_{real}) versus frequency (f). f is the character frequency at which Cimage reaches the maximum and the time constant ($\tau = 1/f$) is the characteristic of the rate capability. As a result, the time constant was estimated to be 1 s, which indicated good power delivery ability. Galvanostatic charge-discharge is a well-accepted method to evaluate the energy storage capability of supercapacitor electrodes. Figure 4d

Shows the galvanostatic charge-discharge curves at different current densities over the voltage window of 0-0.8 V. The linear voltage versus time profile, the symmetrical charge and discharge feature as well as the quick current-voltage response indicated good electrochemical performance of HAPC-11-900 electrode. According to the charge-discharging curves, the specific capacitance, which was calculated based on the total mass of electrode, was 286 F g^{-1} at 0.25 A g^{-1}; and it remained 141 F g^{-1} at a current density of 10 A g^{-1} (Figure 4e). The cycling stability of the HAPC-11-900 electrode was tested by the charge-discharge at 4 A g^{-1} over 2000 cycles (Figure S12). After 2000 cycles, the specific capacitance was reduced from 179 F g^{-1} to 160 F g^{-1}, keeping a high capacitance retention of 89.4%. The Ragone plot shows the dependence of energy density upon the power density (Figure 4f). The two-electrode symmetric supercapacitor exhibited an energy density of 13 Wh kg^{-1} at a power density of 27 kW kg^{-1}. The result has demonstrated that the electrochemical double layer capacitor based on the meso-microporous activated carbon electrode (HAPC-11-900) was able to deliver a relatively high energy density at a high power density. A lot of high performance porous carbon-based supercapacitor electrodes have been reported previously. For example, a hierarchical porous carbon electrode has achieved an energy density of 18.7 Wh kg^{-1} at a power density of 11.0 kW kg^{-1}.[46] An energy density of 1.0 Wh kg^{-1} at a power density of 14.4 kW kg^{-1} has been reported for the activated carbon-coated carbon nanotubes,[47] and an energy density of 12.5 Wh kg^{-1} at a power density of 17 kW kg^{-1} was observed for the glucose-derived micropores carbon.[48] The carbon electrode in this study has exhibited comparable or better electrochemical performance.

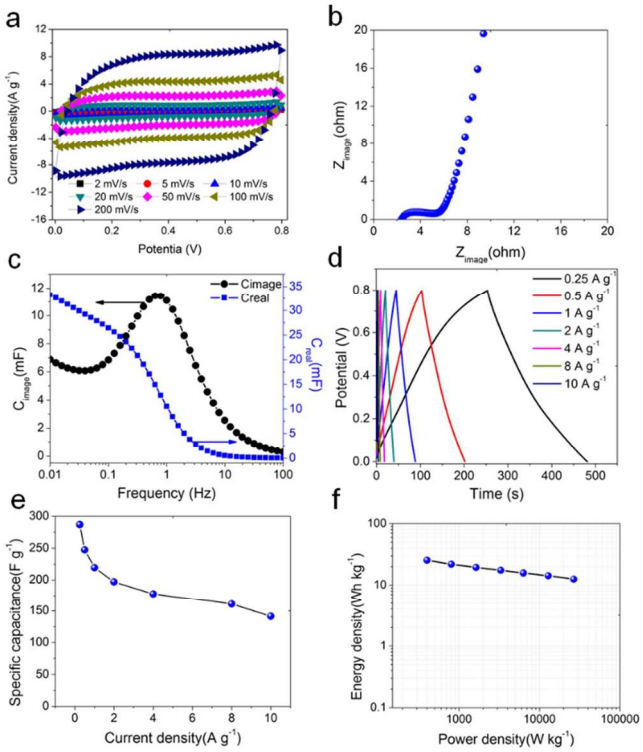

Figure 4. Electrochemical performance of the meso-microporous activated carbon electrode (HAPC-11-900) in a two-electrode cell in the 6 M KOH aqueous electrolyte. (a) CV profiles, (b) Nyquist plot, (c) imaginary capacitance (Cimage) and real capacitance (Creal) versus frequency, (d) charge-discharge curves at different current densities, (e) specific capacitance as a function of the current density derived from the charge-discharge test, and (f) Ragone plot showing the energy density versus the power density.

Conclusions

In summary, a meso-microporous activated carbon was prepared via the template-assisted synthetic method and chemical activation using renewable cellulose and biowaste lignosulphonate as the precursors. Regeneration of cellulose and use of a silica template were two key steps for creating large specific surface area and specific mesopore volume. The chemical activation process was able to adjust the specific micropore volume and the specific mesopore volume. Increasing the micropore volume increased the specific capacitance of carbon electrode while increasing the mesopore volume increased the rate capability. The optimal two-electrode symmetric supercapacitor built on the meso-microporous activated carbon electrode exhibited a specific capacitance of 286 F g-1 at 0.25 A g-1 in the 6 M KOH aqueous electrolyte. The supercapacitor showed an energy density of 13 Wh kg-1 at a power density of 27 kW kg-1.

Acknowledgements

This work is partially supported by an URS grant under the U. S. DOE/ENTL contract (4000.5.682.998.001B). The use of the WVU Shared Facility is appreciated. The authors are grateful for the financial support by the National Natural Science Foundation of China (Grant No. 51372142), Innovation Research Group (IRG: 51321091) and the "100 Talents Program" of the Chinese Academy of Sciences.

Notes and references

[a] State Key Laboratory of Crystal Materials, Shandong University, Jinan 250100, China

[b] Department of Mechanical and Aerospace Engineering, West Virginia University, Morgantown, West Virginia 26505-6106, United State of America

[c] National Energy Technology Laboratory, US Department of Energy, 3610 Collins Ferry Road, Morgantown, West Virginia 26507, United State pf America

* Corresponding authors. Email: hongliu@sdu.edu.cn,

Nick.Wu@mail.wvu.edu (N. Q. Wu)

Electronic Supplementary Information (ESI) available: [details of any supplementary information available should be included here]. See DOI: 10.1039/b000000x/

1. E. Karden, S. Ploumen, B. Fricke, T. Miller and K. Snyder, *Journal of Power Sources*, 2007, **168**, 2-11.
2. C. Abbey and G. Joos, *Industry Applications, IEEE Transactions on*, 2007, **43**, 769-776.
3. J. R. Miller and P. Simon, *Science*, 2008, **321**, 651-652.
4. K. Jost, D. Stenger, C. R. Perez, J. K. McDonough, K. Lian, Y. Gogotsi and G. Dion, *Energy & Environmental Science*, 2013, **6**, 2698-2705.
5. L. L. Zhang and X. S. Zhao, *Chemical Society reviews*, 2009, **38**, 2520-2531.
6. L. Sun, C. Tian, M. Li, X. Meng, L. Wang, R. Wang, J. Yin and H. Fu, *Journal of Materials Chemistry A*, 2013, **1**, 6462-6470.
7. L. Wei and G. Yushin, *Carbon*, 2011, **49**, 4830-4838.
8. M. Genovese, J. Jiang, K. Lian and N. Holm, *Journal of Materials Chemistry A*, 2015.
9. P. Hao, Z. H. Zhao, J. Tian, H. D. Li, Y. H. Sang, G. W. Yu, H. Q. Cai, H. Liu, C. P. Wong and A. Umar, *Nanoscale*, 2014, **6**, 12120-12129.
10. Y. K. Lv, L. H. Gan, M. X. Liu, W. Xiong, Z. J. Xu, D. Z. Zhu, D. S. Wright, *J. Power Sources*, 2012, **209**, 152-157.
11. M. J. Zhi, F. Yang, F. K. Meng, M. Q. Li, A. Manivannan and N. Q. Wu, *Acs Sustain Chem Eng*, 2014, **2**, 1592-1598.
12. D. Klemm, B. Heublein, H. P. Fink and A. Bohn, *Angewandte Chemie*, 2005, **44**, 3358-3393.
13. S. Srivastava, A. Singh and A. Sharma, *Environmental technology*, 1994, **15**, 353-361.
14. H. Zhu, Z. Jia, Y. Chen, N. Weadock, J. Wan, O. Vaaland, X. Han, T. Li and L. Hu, *Nano letters*, 2013, **13**, 3093-3100.
15. Z. Gui, H. Zhu, E. Gillette, X. Han, G. W. Rubloff, L. Hu and S. B. Lee, *ACS Nano*, 2013, **7**, 6037-6046.
16. L. B. Hu, G. Y. Zheng, J. Yao, N. A. Liu, B. Weil, M. Eskilsson, E. Karabulut, Z. C. Ruan, S. H. Fan, J. T. Bloking, M. D. McGehee, L. Wagberg and Y. Cui, *Energy & Environmental Science*, 2013, **6**, 513-518.
17. P. Carrott and M. Ribeiro Carrott, *Bioresource technology*, 2007, **98**, 2301-2312.
18. C. Pelekani and V. L. Snoeyink, *Water Research*, 1999, **33**, 1209-1219.
19. M. Zhi, C. Xiang, J. Li, M. Li and N. Wu, *Nanoscale*, 2013, **5**, 72-88.
20. J. R. Barnett and V. A. Bonham, *Biological reviews of the Cambridge Philosophical Society*, 2004, **79**, 461-472.
21. J. Cai, S. Kimura, M. Wada, S. Kuga and L. Zhang, *ChemSusChem*, 2008, **1**, 149-154.
22. G. E. Fredheim and B. E. Christensen, *Biomacromolecules*, 2003, **4**, 232-239.
23. M. Alonso, M. Oliet, F. Rodriguez, G. Astarloa and J. Echeverría, *Journal of Applied Polymer Science*, 2004, **94**, 643-650.
24. G. Van der Klashorst, C. Forbes and K. Psotta, *Holzforschung-International Journal of the Biology, Chemistry, Physics and Technology of Wood*, 1983, **37**, 279-286.
25. P. Simon and Y. Gogotsi, *Nat Mater*, 2008, **7**, 845-854.
26. M. X. Liu, J. S. Qian, Y. H. Zhao, D. Z. Zhu, L. H. Gan and L. W. Chen, *J. Mater. Chem. A*, 2015, **3**, 11517-11526.
27. M. X. Liu, L. H. Gan, F. Q. Zhao, H. X. Xu, X. Z. Fan, C. Tian, X. Wang, Z. J. Xu, Z. X. Hao and L. W. Chen, *Carbon*, 2007, **45**, 2710-2712.
28 M. X. Liu, L. H. Gan, C. Tian, J. C. Zhu, Z. J. Xu, Z. X. Hao and L. W. Chen, *Carbon*, 2007, **45**, 3045-3046.
29. W. Xiong, M. X. Liu, L. H. Gan, Y. K. Lv, Y. Li, L. Yang, Z. J. Zhu, Z. X. Hao, H. L. Liu and L. W. Chen, *J. Power Sources*, 2011, 196, 10461-10464.
30. Y. H. Zhao, M. X. Liu, L. H. Gan, X. M. Ma, D. Z. Zhu, Z. J. Xu and L. W. Chen, Energy Fuels, 2014, 28, 1561-1568.
31. Y. H. Zhao, M. X. Liu, X. X. Deng, L. Miao, P. K. Tripathi, X. M. Ma, D. Z. Zhu, Z. J. Xu, Z. X. Hao and L. H. Gan, Electrochimica Acta, 2015, 153, 448-455.
32. H. Qi, C. Chang and L. Zhang, *Cellulose*, 2008, **15**, 779-787.
33. X. M. Ma, L. H. Gan, M. X. Liu, P. K. Tripathi, Y. H. Zhao, Z. J. Xu, D. Z. Zhu and L. W. Chen, *J. Mater. Chem. A,* 2014, **2**, 8407-8415.
34. P. K. Tripathi, M. X. Liu, Y. H. Zhao, X. M. Ma, L. H. Gan, O. Noonan and C. Z. Yu, *J. Mater. Chem. A*, 2014, **2**, 8534-8544.
35. M. Thommes, Chemie Ingenieur Technik, 2010, 82, 1059-1073.
36. D. Saha, Y. C. Li, Z. H. Bi, J. H. Chen, J. K. Keum, D. K. Hensley, H. A. Grappe, H. M. Meyer, S. Dai, M. P. Paranthaman and A. K. Naskar, *Langmuir*, 2014, **30**, 900-910.
37. M. Li, S. K. Cushing, X. Zhou, S. Guo and N. Wu, *Journal of Materials Chemistry*, 2012, **22**, 23374-23379.
38. A. C. Ferrari and J. Robertson, *Physical Review B*, 2000, **61**, 14095-14107.
39. M. X. Liu, L. H. Gan, W. Xiong, Z. J. Xu, D. Z. Zhu and L. W. Chen, J. Mater. Chem. A, 2014, 2, 2555-2562.
40. M. X. Liu, L. H. Gan, W. Xiong, F. Q. Zhao, X. Z. Fan, D. Z. Zhu, Z. J. Xu, Z. X. Hao and L. W. Chen, Energy Fuels, 2013, 27, 1168-1173.
41. S. Park, J. O. Baker, M. E. Himmel, P. A. Parilla and D. K. Johnson, *Biotechnology for Biofuels*, 2010, **3**, 10.
42. Y. Q. Liu, L. Gao and J. Sun, *J Phys Chem C*, 2007, **111**, 1223-1229.
43. M. D. Stoller and R. S. Ruoff, *Energy & Environmental Science*, 2010, **3**, 1294.
44. M. Ezekiel, 1930. John Wiley and Sons, 1St Edition.
45. V. Khomenko, E. Frackowiak and F. Béguin, *Electrochimica Acta*, 2005, **50**, 2499-2506.
46. B. You, J. H. Jiang and S. J. Fan, *Acs Appl Mater Inter*, 2014, **6**, 15302-15308.
47. K. Shi, M. Ren and I. Zhitomirsky, *Acs Sustain Chem Eng*, 2014, **2**, 1289-1298.
48. M. Sevilla, L. Yu, C. O. Ania and M. M. Titirici, *ChemElectroChem*, 2014, **1**, 2138-2145.

Graphical Abstract

Lignosulphonate-cellulose Derived Porous Activated Carbon for Supercapacitor Electrode

Zhenhuan Zhao[a,b], Shimeng Hao[b], Pin Hao[a], Yuanhua Sang[a], Ayyakkannu Manivannan[c], Nianqiang Wu[b], Hong Liu[a*]*

[a] State Key Laboratory of Crystal Materials, Shandong University, Jinan 250100, China

[b] Department of Mechanical and Aerospace Engineering, West Virginia University, Morgantown, West Virginia 26505-6106, United State of America

[c] National Energy Technology Laboratory, US Department of Energy, 3610 Collins Ferry Road, Morgantown, West Virginia 26507, United State pf America

* Corresponding authors. Email: hongliu@sdu.edu.cn, Nick.Wu@mail.wvu.edu (N. Q. Wu)